Title: Termite mounds can increase the robustness of dryland ecosystems to climatic change

Authors: Juan A. Bonachela[1†], Robert M. Pringle[1,2], Efrat Sheffer[1], Tyler C. Coverdale[1], Jennifer A. Guyton[1], Kelly K. Caylor[3], Simon A. Levin[1], Corina E. Tarnita[1,2]*

Affiliations:

[1] Department of Ecology & Evolutionary Biology, Princeton University, Princeton, NJ 08544, USA

[2] Mpala Research Centre, P.O. Box 555, Nanyuki, Kenya

[3] Department of Civil & Environmental Engineering, Princeton University, Princeton, NJ 08544, USA

* Correspondence to: ctarnita@princeton.edu

† Current address: juan.bonachela@strath.ac.uk, MASTS Marine Population Modelling Group, Department of Mathematics and Statistics, University of Strathclyde, 26 Richmond Street, Glasgow, G1 1XH, Scotland, United Kingdom.

One Sentence Summary:

Termites shape vegetation patterns in arid landscapes and buffer ecosystems against sudden drought-induced desertification.

Abstract: Self-organized spatial vegetation patterning is widespread and has been described using models of scale-dependent feedback between plants and water on homogeneous substrates. As rainfall decreases, these models yield a characteristic sequence of patterns with increasingly sparse vegetation, followed by sudden collapse to desert. Thus, the final, spot-like pattern may provide early warning for such catastrophic shifts. In many arid ecosystems, however, termite nests impart substrate heterogeneity by altering soil properties, thereby enhancing plant growth. We show that termite-induced heterogeneity interacts with scale-dependent feedbacks to produce vegetation patterns at different spatial grains. Although the coarse-grained patterning resembles that created by scale-dependent feedback alone, it does not indicate imminent desertification. Rather, mound-field landscapes are more robust to aridity, suggesting that termites may help stabilize ecosystems under global change.

Main Text

Over the past decade, many studies have documented large-scale, spatially-periodic clusters of vegetation and other sessile organisms, typically in resource-limited environments (*1-4*). Such patterns, found at many levels of biological organization (*5*), can be described by models of scale-dependent feedback (SDF) coupling short-range activation with long-range inhibition (*3-9*). For example, in arid and semi-arid savannas and grasslands ('drylands'), plants facilitate neighbors by increasing water infiltration while competing for water with distant individuals (*10*). In these models, reducing rainfall generates a predictable sequence of patterns with decreasing overall plant biomass: overdispersed gaps, labyrinths, spots, and finally barren desert. This last transition is known as a 'catastrophic shift,' or sudden collapse to an unvegetated state (*11*, *12*).

The robustness (*sensu* (*13*), also called resilience (*14*)) of drylands to such catastrophic shifts is an urgent concern given the importance of these systems to human livelihoods (drylands cover >40% of Earth's land surface and are home to >38% of the populace (*15*)) and the increased frequency/intensity of drought expected under climate change(*16*). Scientists have therefore proposed using spotted vegetation patterns, readily identifiable in aerial imagery, as 'early-warning signals' of imminent catastrophic shifts (*11*, *12*). However, operationalizing an early-warning system requires mechanistic understanding of both the cause(s) of spotted patterns and the linkage between patterns and robustness; otherwise, 'false alarms' could lead to costly resource misallocation (*17*).

Prior SDF models assume soil homogeneity, but most real ecosystems feature heterogeneous substrates. One globally widespread source of heterogeneity is ecosystem engineering by soil-dwelling macrofauna such as termites, ants, and earthworms. Termites are particularly important in savannas of Africa, Australasia, and South America, and their nest structures ('mounds') shape many environmental properties; analogous structures built by ants and burrowing mammals are similarly influential worldwide (e.g., (*18*)). Mound soils differ from surrounding 'matrix' soils in physical and chemical composition, which enhances vegetation growth (*19*, *20*), creating 'islands of fertility' (*20-22*) (Fig. 1). Moreover, mounds are frequently spatially overdispersed, reflecting competition among neighboring colonies (*20-25*), thereby creating spotted vegetation patterns (Fig. 1). The resemblance of these patterns to those predicted by SDF has been noted (*4*, *10*) but not formally analyzed. Importantly, these two patterning mechanisms are not mutually exclusive and may co-occur.

We modeled SDF on a template of overdispersed termite mounds and tested results against imagery from semi-arid savanna at Kenya's Mpala Research Centre (MRC). Mounds in this system—lenticular humps with belowground chambers and passages (*21*)—are built by fungus-cultivating termites (Macrotermitinae: *Odontotermes*), common throughout the Paleotropics. However, our results are applicable to mounds of diverse species and architectures, provided nutrient and/or water availability is elevated either on the mound-proper or in the annular zone around the mound.

We adapt a well-studied three-variable SDF model (*10*) that describes the spatiotemporal dynamics of aboveground vegetation biomass as a function of rainfall (partitioned into runoff

and soil water) (*10*, *23*). In traditional two-component SDF models, short-distance enhancement leading to pattern formation usually arises from autocatalysis (positive-feedback) in an 'activator' species (*8*, *9*). When more than two components interact, as in the model employed here, enhancement can arise indirectly through autocatalytic feedback loops (here: plants—soil water), generating similar pattern morphologies (*26*). We include termite-mound effects in the model by modifying just two parameters. One is the conversion factor c, the efficiency with which plants convert water into biomass ('water-use efficiency'), which we assume is mediated by elevated nutrient availability on mounds (*19*, *27*). The other is the half-saturation constant of water infiltration, k_2, which we modify to account for termites' creation of macropores and alteration of soil texture (*19*, *28*). We leave all other parameters unchanged (Table S1) to enable comparison with prior work.

We assume that both nutrient-mediated water-use efficiency and infiltration are elevated on mounds (Fig. S1), consistent with prior research; specifically, we explore a likely range of on- *versus* off-mound increases of 0-67% for infiltration and 0-50% for water-use efficiency (*20*, *23*, *29*). We further assume that termites' effects on water-use efficiency (but not infiltration) are zero-sum: i.e., termites concentrate nutrients on mounds (*27*), but do not increase net nutrient content of the system (this is conservative in terms of finding beneficial effects of termites, and we analyze alternative scenarios in the Supplementary Material (*23*)). Finally, to assess the effects of rainfall variability, we incorporate seasonality and stochasticity in rainfall based on MRC rainfall records (Fig. 2A).

This modified model yields greater on- than off-mound vegetation biomass (Fig. 2B). Two types of pattern can be identified. One is a coarse-grained lattice of overdispersed vegetation hotspots, reflecting the underlying distribution of termite mounds (*21*), which is exogenous to our model, in conjunction with mounds' positive effects on plant biomass, which is predicted by our model and confirmed with field data from MRC (*23*) (Fig. 2C). The other comprises fine-grained regularity of mound and matrix vegetation resulting from SDF (Fig. 2D,E). The wavelengths of the fine-grained pattern, both on and off mounds, are determined by local dispersal of plants and diffusion of soil and surface water (*30*) and depend on the values of water-use efficiency and infiltration: greater values increase vegetation homogeneity; lower values yield regular gaps, labyrinths, and spots, as found in prior SDF models. Thus, the greater the termite-induced improvements in water-use efficiency and infiltration, the more divergent the on- *versus* off-mound patterning (Figs. 2D, S6). These fine-grained patterns are insensitive to mound distribution (we find equivalent patterns for a single mound and square or hexagonal arrangements), and off-mound patterning is largely insensitive to mound proximity (Fig. S3). Finally, our model produces a 'halo' of barren soil at mound edges, resulting from the highly vegetated mound acting as a sink for nearby water, matching observations from various African savannas (Fig. 1B,D).

To evaluate model predictions of fine-grained patterning, we used Fourier transforms to analyze low-altitude (10m) aerial photographs of matrix vegetation from MRC (Fig. 3A-C) (*23*). Off-mound, we find spotted patterns with ~20-cm wavelength, closely matching the simulated pattern (Fig. 3D,E). Moreover, as predicted, mound vegetation is both denser (*23*) and more evenly distributed than matrix vegetation (Fig. S8). Thus, incorporating termite-induced soil heterogeneity in the SDF framework gives a realistic description of observed patterning. Exact quantitative correspondence is not expected, because our analysis uses generic parameter values

from prior work (*10*). This model could be further extended to include interactions among plant types (e.g., trees vs. grasses) and/or herbivore impacts, and its predictions tested using rain-out/watering experiments.

We next use the modified model to analyze the system's robustness (*13*) to precipitation changes. We consider two components of robustness: 'resistance' to perturbation and 'recovery' from an undesirable stable state. We find that termite mounds increase ecosystem robustness in three ways (Fig. 4). They enhance resistance, enabling vegetation to persist under substantially reduced rainfall; they reduce the rainfall threshold required for recovery from desert; and they make desertification more gradual (i.e., less catastrophic), and thus easier to anticipate and ameliorate. These changes occur because improved infiltration and water-use efficiency on-and-around mounds enable plants to persist, and to repopulate following extirpation, under more arid conditions: mounds act as refugia for vegetation after the matrix has collapsed to desert.

Sufficient improvement of either water-use efficiency or infiltration can independently increase robustness. As rainfall *decreases*, two sudden drops in biomass occur (Figs. 4B, S4-5). The first ('i' in Fig. 4B) represents loss of matrix vegetation only and corresponds to total desertification in the system without mounds ('i' in Fig. 4A). The second ('ii') represents loss of vegetation from mounds (and hence the entire system) and occurs at lower rainfall, indicating enhanced *resistance*. As rainfall *increases* from zero, two sudden jumps in biomass occur (Figs. 4B, S4-5): revegetation of mounds occurs first, at lower rainfall, followed by revegetation of the matrix, indicating enhanced *recovery*. Insufficient termite-induced improvements yield only one shift, as occurs in the absence of mounds (*10*), and do not enhance ecosystem robustness (Fig. S5); in this case, on- and off-mound trajectories are similar. Improving either parameter yields comparable effects, but for our parameter regions, water-use efficiency contributes more to robustness than does infiltration (Fig. S5).

This model describes annual-to-decadal temporal scales, over which precipitation influences the dynamics of vegetation, but not the mounds (*23*). Thus, the model captures pattern evolution and sudden transitions in response to climate-change-induced pulses of drought and rainfall, but may not apply if sustained (>50-year) reductions in baseline precipitation cause termite extinction and subsequent homogenization of mound structures. Future theoretical and empirical work is needed to elucidate longer-term dynamic feedbacks between vegetation and mound construction, distribution, and decay.

Our analysis shows that when SDF occurs on a template of overdispersed mounds created by ecosystem engineers, two distinct types of regular patterning coexist at different scales. The fine-grained SDF-generated patterns documented here may be common, but previously unreported because (a) they cannot be observed in available satellite imagery; (b) even at lower altitudes, grass canopies obscure patterns with centimeters-scale wavelengths; and (c) stochastic rainfall decreases apparent regularity (compare Fig. 2 and Movies S1-2 with Fig. S3, which assumes constant rainfall). The simplest SDF scenarios typically produce patterns with a single characteristic wavelength (*3*), whereas models combining multiple mechanisms can show complex patterns (*31*, *32*). Thus, co-occurrence of patterns with distinct wavelengths may be a general indicator that multiple mechanisms are operating simultaneously. The mound—SDF interaction is one such route to pattern coexistence, and is likely common worldwide because it does not depend on specific mound attributes. Appropriately modified models might therefore

inform ongoing debates in which SDF and soil macrofauna are considered alternative hypotheses for particular large-scale patterns, such as Namibian 'fairy circles' (*33*, *34*) and various 'mima-like mounds' worldwide (*35*).

We further conclude that termites, by creating refugia for plants and nuclei for revegetation, can enhance drylands' resistance to and recovery from drought. These islands of fertility (*20*) appear spot-like in remotely sensed imagery (Fig. 1), but unlike SDF-generated spots they indicate robustness rather than vulnerability to collapse. These findings confirm the critical links between remotely-sensed patterns and ecosystem dynamics, but qualify the use of remotely-sensed patterning to predict catastrophic shifts. Similar phenomena may occur in other systems where vegetation patterning is governed by mechanisms generating apparent SDF dynamics, such as banded vegetation arising from runoff induced by biological crusts on arid hillslopes (*4*, *36*). By such engineering of soil, termites and other ecosystem engineers may buffer the effects of anthropogenic global change in some of the world's most environmentally and socio-economically sensitive regions.

References and Notes

1. C. A. Klausmeier, *Science* **284**, 1826–1828 (1999).

2. J. van de Koppel *et al.*, *Science* **322**, 739–742 (2008).

3. M. Rietkerk, J. van de Koppel, *TREE* **23**, 169–175 (2008).

4. V. Deblauwe, P. Couteron, O. Lejeune, J. Bogaert, N. Barbier, *Ecography* **34**, 990–1001 (2011).

5. H. Meinhardt, *Nature* **376**, 722–723 (1995).

6. S. A. Levin, L. A. Segel, *SIAM Review* **27**, 45–67 (1985).

7. E. Meron, *Math. Model. Nat. Phenom.* **6**, 163–187 (2011).

8. A. Gierer, H. Meinhardt, *Kybernetik* **12**, 30–39 (1972).

9. P. K. Maini, K. J. Painter, H. Nguyen Phong Chau, *Faraday Trans.* **93**, 3601–3610 (1997).

10. M. Rietkerk *et al.*, *Am. Nat.* **160**, 524–530 (2002).

11. M. Scheffer *et al.*, *Nature* **461**, 53–59 (2009).

12. M. Rietkerk, S. C. Dekker, P. C. de Ruiter, J. van de Koppel, *Science* **305**, 1926–1929 (2004).

13. S. A. Levin, J. Lubchenco, *BioScience* **58**, 27 (2008).

14. C. S. Holling, *Annu. Rev. Ecol. Evol. Syst.*, 1–23 (1973).

15. J. F. Reynolds *et al.*, *Science* **316**, 847–851 (2007).

16. N. S. Diffenbaugh, C. B. Field, *Science* **341**, 486–492 (2013).

17. V. Dakos, S. Kéfi, M. Rietkerk, E. H. van Nes, M. Scheffer, *Am. Nat.* **177**, E153–E166 (2011).

18. C. Alba-Lynn, J. K. Detling, *Oecologia* **157**, 269–278 (2008).

19. P. Jouquet, S. Traoré, C. Choosai, C. Hartmann, D. Bignell, *Eur J Soil Biol* **47**, 215–222 (2011).

20. G. W. Sileshi, M. A. Arshad, S. Konaté, P. O. Nkunika, *J Veg Sci* **21**, 923–937 (2010).

21. R. M. Pringle, D. F. Doak, A. K. Brody, R. Jocqué, T. M. Palmer, *PLoS Biol* **8**, e1000377 (2010).

22. A. B. Davies *et al.*, *Ecography*, 1–11 (2014).

23. See supplementary materials on Science Online.

24. J. Korb, K. E. Linsenmair, *Oecologia* **127**, 324–333 (2001).

25. S. R. Levick *et al.*, *Nat Comm* **1**, 1–7 (2010).

26. R. A. Satnoianu, M. Menzinger, P. K. Maini, *J Math Biol* **41**, 493–512 (2000).

27. C. L. Seymour *et al.*, *Soil Biol Biochem* **68**, 95–105 (2014).

28. N. Bottinelli *et al.*, *Soil Till Res*, 1–7 (2014).

29. A. Mando, L. Stroosnijder, L. Brussaar, *Geoderma* **74**, 107–113 (1996).

30. E. Sheffer, J. von Hardenberg, H. Yizhaq, M. Shachak, E. Meron, *Ecol. Lett.* **16**, 127–139 (2012).

31. K. M. Page, P. K. Maini, N. A. Monk, *Physica D* **202**, 95–115 (2005).

32. Q.-X. Liu *et al.*, *Nat Comm* **5**, 5234 (2014).

33. N. Juergens, *Science* **339**, 1618–1621 (2013).

34. S. Getzin *et al.*, *Ecography*, 1–11 (2014).

35. M. D. Cramer, N. N. Barger, *Palaeogeogr Palaeocl* **409**, 72–83 (2014).

36. O. Malam Issa, J. Trichet, C. Défarge, A. Couté, C. Valentin, *Catena* **37**, 175–196 (1999).

37. P. M. Ahn, L. C. Geiger, *Ministry of Agriculture, National Agricultural Laboratories,*

Kabete, Kenya (1987).

38. T. P. Young, B. D. Okello, D. Kinyua, T. M. Palmer, *African Journal of Range and Forage Science* **14**, 94–102 (1997).

39. J. Darlington, *Sociobiology* **45**, 521–542 (2005).

40. J. P. Darlington, *Oecologia* **66**, 116–121 (1985).

41. J. Darlington, R. Bagine, *Sociobiology* **33**, 215–225 (1999).

42. K. Fox-Dobbs, D. F. Doak, A. K. Brody, T. M. Palmer, *Ecology* **91**, 1296–1307 (2010).

43. T. M. Palmer, *Ecology* **84**, 2843–2855 (2003).

44. A. K. Brody, T. M. Palmer, K. Fox-Dobbs, D. F. Doak, *Ecology* **91**, 399–407 (2010).

45. J. Darlington, *Insect. Soc.* **44**, 393–408 (1997).

46. P. Eggleton, in *Termites: Evolution, Sociality, Symbioses, Ecology*, T. Abe, Ed. (Kluwer Academic Publishers, 2000), pp. 25–51.

47. J. Korb, in D. E. Bignell, Y. Roisin, N. Lo, Eds. (Springer Netherlands, Dordrecht, 2010), pp. 349–373.

48. E. J. Gabet, O. J. Reichman, E. W. Seabloom, *Annu. Rev. Earth Planet. Sci.* **31**, 249–273 (2003).

49. W. A. Macfadyen, *Geographical Journal*, 199–211 (1950).

50. P. E. Glover, E. C. Trump, L. Wateridge, *The Journal of Ecology*, 367–377 (1964).

51. D. Pomeroy, *Journal of East African Natural History* **94**, 319–341 (2005).

52. C. Grohmann, J. Oldeland, D. Stoyan, K. E. Linsenmair, *Insect. Soc.* **57**, 477–486 (2010).

53. G. Schuurman, J. M. Dangerfield, *J. Trop. Ecol.* **13**, 39–49 (1997).

54. A. V. Spain, D. F. Sinclair, P. J. Diggle, *Acta oecologica. Oecologia generalis* **7**, 335–352 (1986).

55. T. A. Gontijo, D. J. Domingos, *J. Trop. Ecol.* **7**, 523–529 (1991).

56. T. Bourguignon, M. Leponce, Y. Roisin, *Ecological Entomology* **36**, 776–785 (2011).

57. N. Waloff, R. E. Blackith, *The Journal of Animal Ecology*, 421–437 (1962).

58. R. Boulay *et al.*, *Ecology* **91**, 3312–3321 (2010).

59. S. C. Levings, N. R. Franks, *Ecology*, 338–344 (1982).

60. R. T. Ryti, T. J. Case, *Oecologia* **69**, 446–453 (1986).

61. J. H. Cushman, G. D. Martinsen, A. I. Mazeroll, *Oecologia* **77**, 522–525 (1988).

62. H. Laurie, *South African journal of science* **98**, 141–146 (2002).

63. L. C. R. Silva, G. D. Vale, R. F. Haidar, L. da S L Sternberg, *Plant Soil* **336**, 3–14 (2010).

64. D. Renard *et al.*, *Plant Soil* **351**, 337–353 (2011).

65. J. M. Moore, M. D. Picker, *Oecologia* **86**, 424–432 (1991).

66. J. J. Midgley, C. Harris, H. Hesse, A. Swift, *South African journal of science* **98**, p. 202–204 (2002).

67. N. Z. Elkins, G. V. Sabol, T. J. Ward, W. G. Whitford, *Oecologia* **68**, 521–528 (1986).

68. K. E. Lee, R. C. Foster, *Aust. J. Soil Res.* **6**, 745–775 (1991).

69. J. Léonard, J. L. Rajot, *Geoderma* **104**, 17–40 (2001).

70. W. Ehlers, *Soil Science* **119**, 242–249 (1975).

71. R. M. Holdo, L. R. McDowell, *Biotropica* **36**, 231–239 (2004).

72. J. P. Loveridge, S. R. Moe, *J. Trop. Ecol.* **20**, 337–343 (1999).

73. P. Jouquet, V. Tavernier, L. Abbadie, L. Michel, *African Journal of Ecology* **43**, 191–196 (2005).

74. C. C. Grant, M. C. Scholes, *Biological Conservation* **130**, 426–437 (2006).

75. J. Darlington, R. D. Dransfield, *Insect. Soc.* **34**, 165–180 (1987).

76. E. W. Jones, *The Journal of Ecology*, 83–117 (1956).

77. J. P. Watson, *The Journal of Ecology* **55**, 663–669 (1967).

78. F. R. Smith, R. I. Yeaton, *Plant Ecol* **137**, 41–53 (1998).

79. C. M. Gosling, J. P. G. M. Cromsigt, N. Mpanza, H. Olff, *Ecosystems* **15**, 128–139 (2011).

80. H. Meinhardt, *Developmental Biology* **157**, 321–333 (1993).

81. W. S. W. Trollope, A. L. F. Potgieter, *J. Grassl. Soc. Sth Afr.* **4**, 148–152 (1986).

82. M. A. Mugglestone, E. Renshaw, *Computers and Geoscience* **24**, 771–784 (1998).

83. P. Couteron, O. Lejeune, *J Ecology* **89**, 616–628 (2001).

84. N. Barbier, P. Couteron, J. Lejoly, V. Deblauwe, O. Lejeune, *J Ecology* **94**, 537–547 (2006).

Acknowledgments: The data are located on the Dryad Digital Repository. This research was supported by grants from the National Science Foundation (DEB-1355122 to CET, RMP, and DF Doak), the Princeton Environmental Institute (Grand Challenges grant to RMP and CET), the Andrew W. Mellon Foundation ("Dynamics of South African Vegetation" to SAL), the John Templeton Foundation (FQEB RFP-12-14 to CET and SAL). We thank: the Government of Kenya for permission to conduct research; I. Cuesta, L. Hedin, R. Martinez-Garcia, J.D. Murray, and T.P. Young for helpful discussions; and T.P. Young, C. Riginos, and K. Veblen for access to the Kenya Long-term Exclosure Experiment (KLEE), funded by NSF LTREB 12-56034. We thank K. Grabowski and M. Mohamed for assistance in the field.

Author Contributions: CET conceived the study; CET, RMP and JAB developed the theory; JAB analyzed the model; ES performed the analysis of pattern in imagery and its comparison with simulation results; RMP, TCC, and JAG collected field data; SAL, KKC and ES contributed to discussions of the modeling and analysis; CET, RMP and JAB wrote the first draft of the manuscript; all authors contributed revisions.

Figures

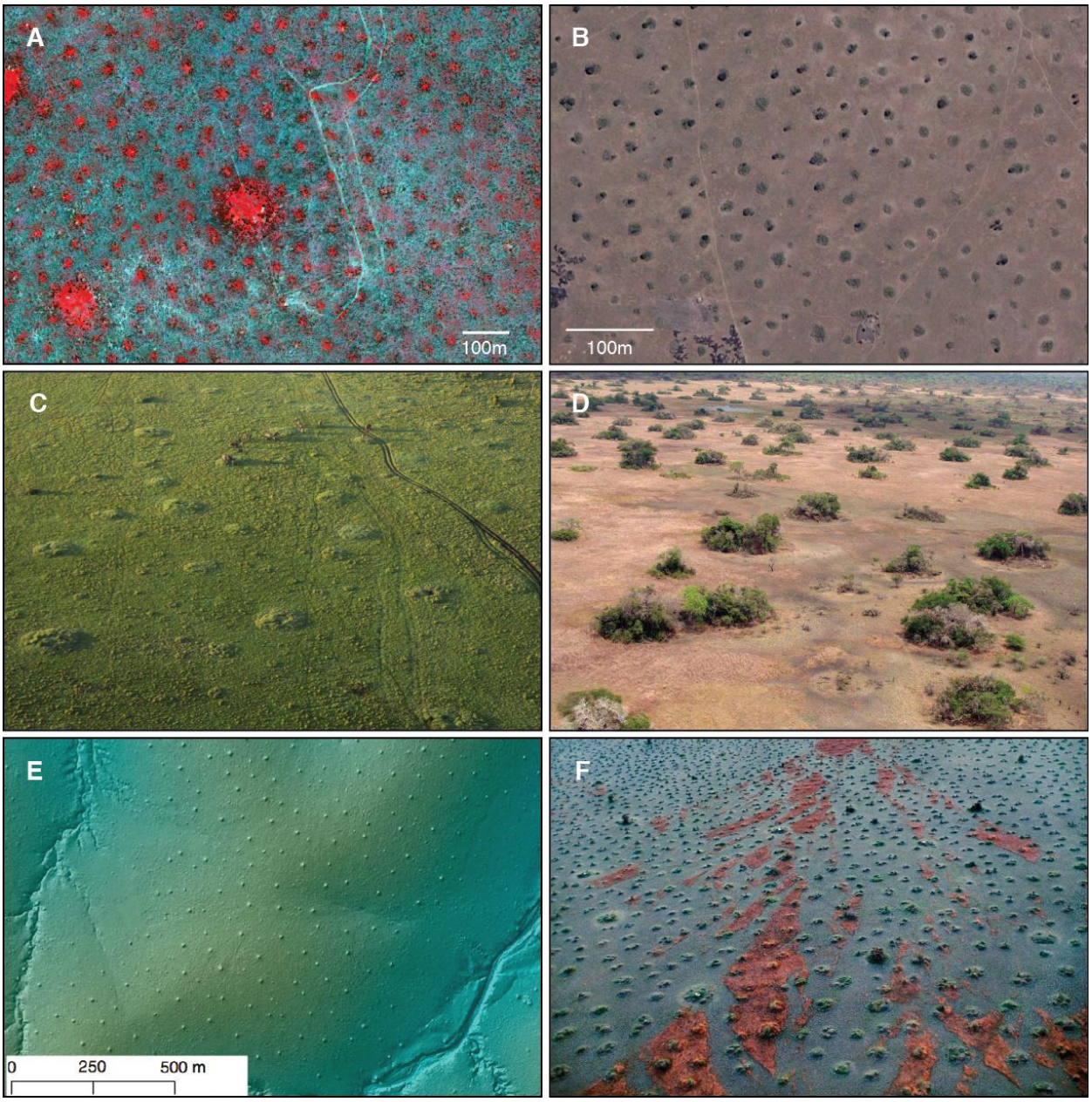

Fig. 1. **Patterned termite mounds in real ecosystems. (A)** False-color infrared Quickbird satellite image (2.4-m resolution) of termite mounds at MRC; mounds appear as small red spots, indicating high primary productivity (larger red patches are abandoned cattle corrals). **(B)** Presumed termite mounds in northwestern Tanzania (-1.29158 latitude, 34.37146 longitude) identified using Google Earth (2006 image © DigitalGlobe); note barren halos around many mounds. **(C)** Grass-dominated mounds in Kenya's Masai Mara, taken from hot-air balloon; see elephants for scale. (D) Tree-dominated mounds in Sofala, Mozambique, taken from light aircraft. **(E)** LiDAR hillshade image of termite mounds in South Africa's Kruger National Park, from (*25*). **(F)** Termite mounds on Bangweulu floodplain, Zambia (image courtesy of Frans Lanting).

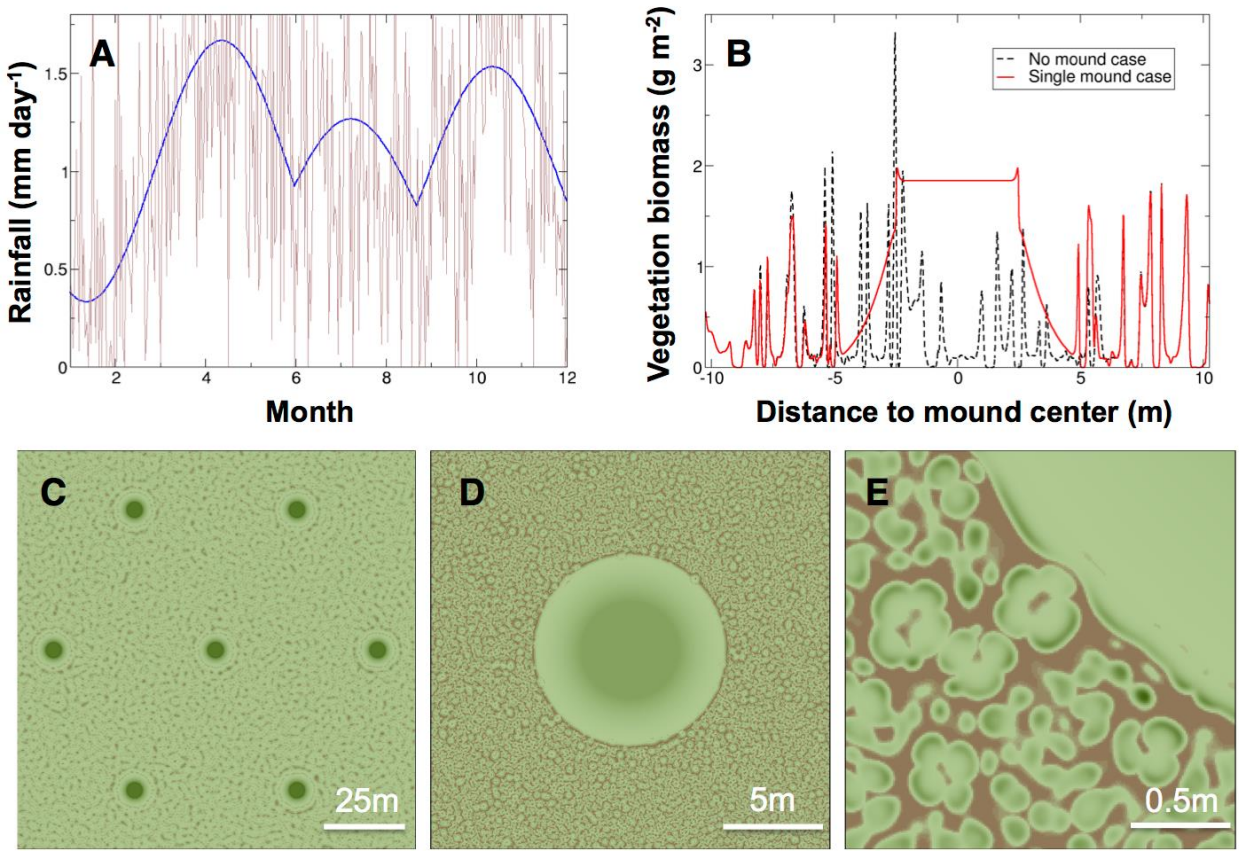

Fig. 2. Vegetation patterns obtained with stochastic rainfall and termite-induced heterogeneity. (A) Stochastic rainfall (brown curve) based on observed mean-monthly rainfall (blue curve) at MRC, 1999-2013. **(B)** Transect of predicted vegetation biomass density through a mound (solid curve) and in the absence of mounds (dashed curve). **(C-E)** Model outputs showing **(C)** 123x123m region encompassing seven hexagonally distributed mounds; **(D)** 20.5x20.5m region with only one mound, showcasing halo effect (cf. Fig 1B,D); **(E)** 2x2m region showing patchy off-mound vegetation and homogeneous on-mound vegetation. Green = vegetation; brown = soil. Darker green regions have higher biomass. See table S1 for parameterization.

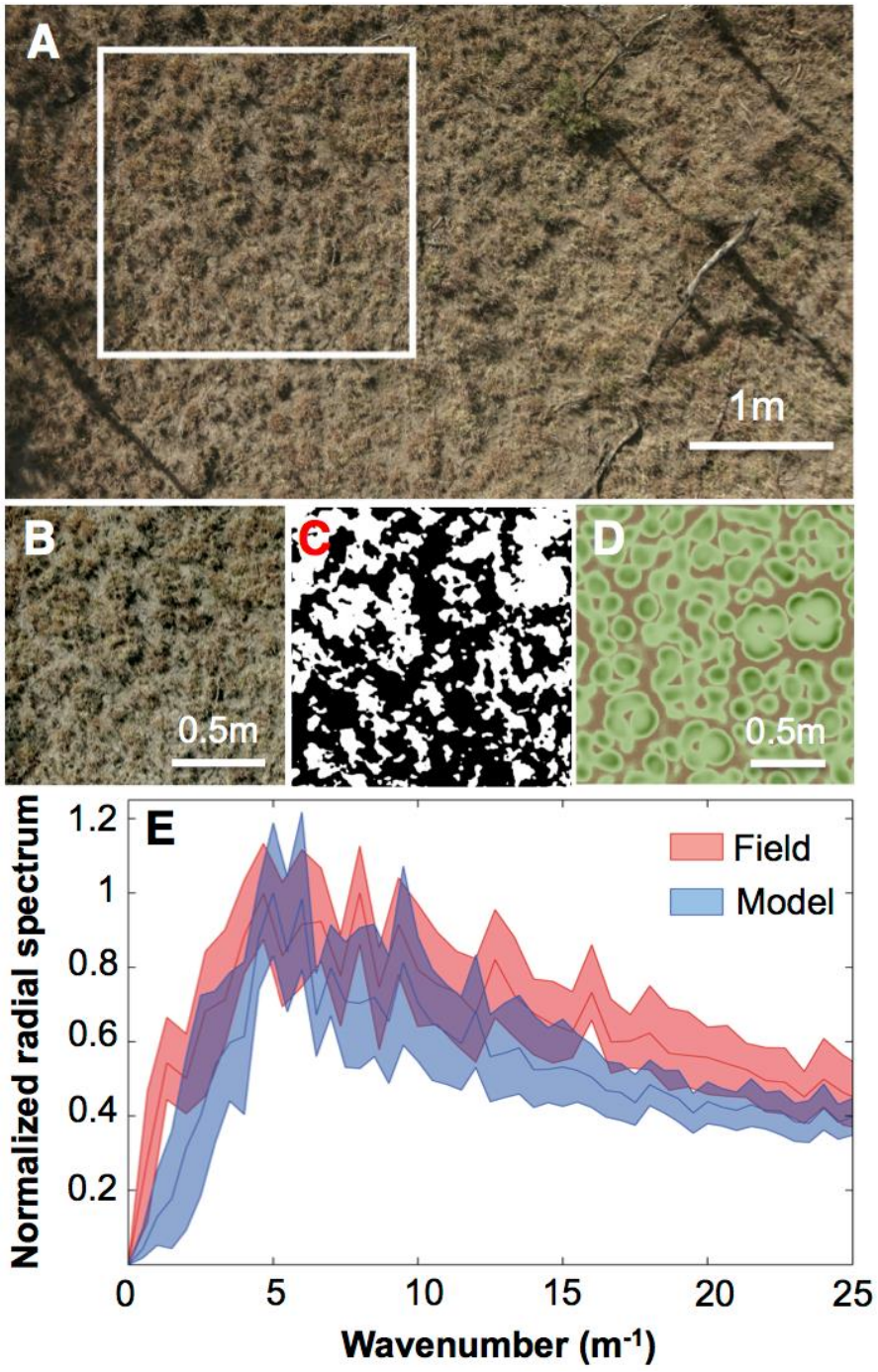

Fig. 3. Correspondence of predicted and observed vegetation patterns. (A) Photograph of 3.5x6m region of matrix vegetation taken from 10m height; **(B)** 1.5x1.5m section used in the analysis, from white square in (A); **(C)** binary (white = vegetation, black = soil) transformation of panel (B); **(D)** model output used for comparison, with parameterization as in Fig. 2. **(E)** Normalized radial spectrum of real images (*n*=14) and model simulations (*n*=192), as a function of wavenumber.

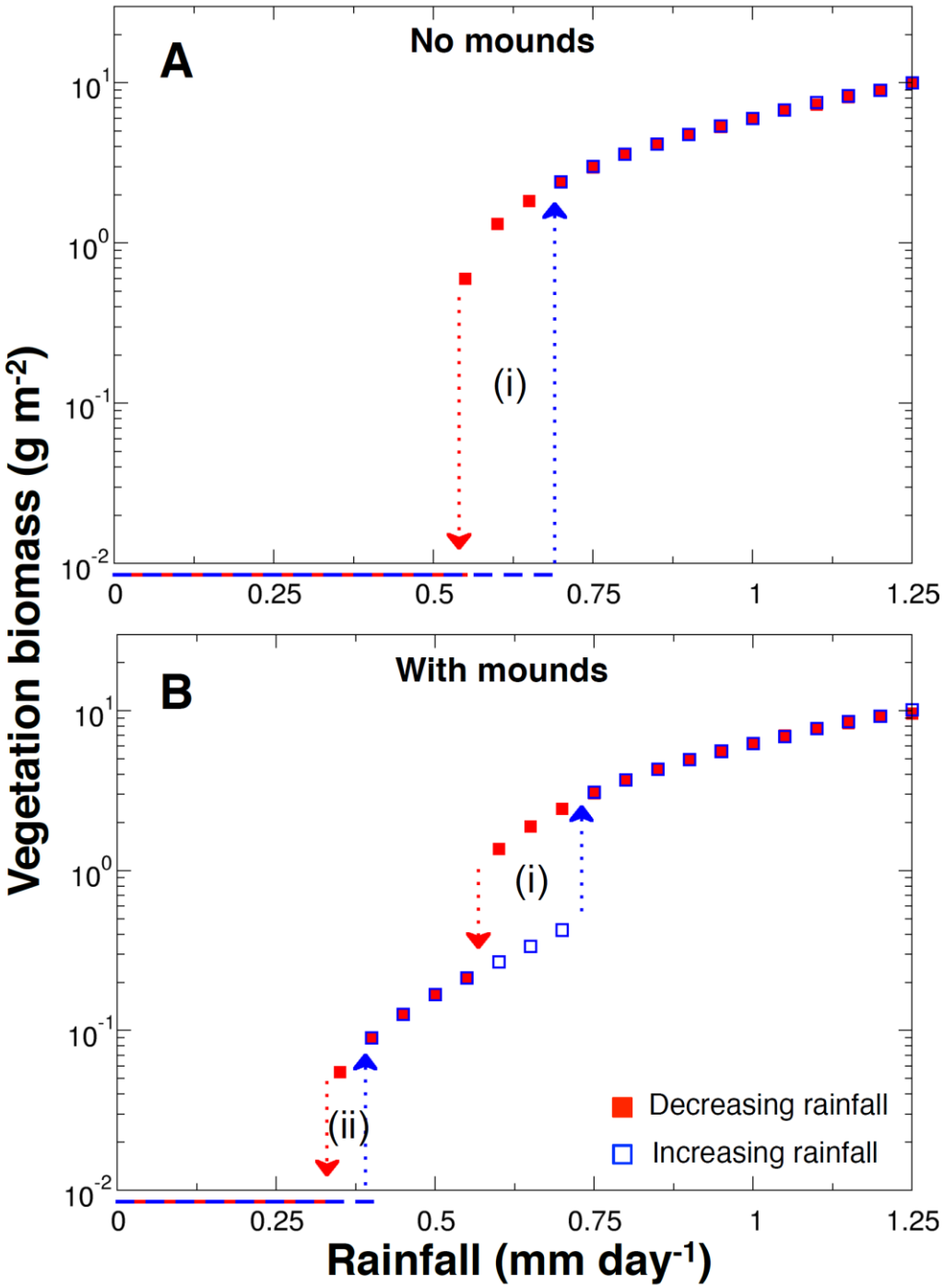

Fig. 4. Termite mounds increase ecosystem robustness. Semi-logarithmic phase diagrams under increasing (blue) and decreasing (red) rainfall for **(A)** model with no termite mounds and **(B)** the modified model with 50% on-mound versus off-mound improvement in both growth rate and infiltration efficiency. Without mounds, one hysteresis cycle occurs (i), corresponding to sudden transitions to and from desertification; adding mounds gives two hysteresis cycles, corresponding to loss/recovery of matrix vegetation (i) and total desertification/revegetation (ii). For both panels, we used fixed rainfall rates and parameters from table S1 and Fig. S5.

Supplementary Materials:

Supplementary text

Figures S1-S8

Tables S1

Movies S1-S2

References (*37-84*)